RSC Advances

ROYAL SOCIETY OF CHEMISTRY

www.rsc.org/advances

Journal Name

COMMUNICATION

High Performance Nanoporous Silicon Photoelectrodes co-catalyzed with Earth Abundant $[Mo_3S_{13}]^{2-}$ Nanocluster via Drop Coating

Received 00th January 20xx,
Accepted 00th January 20xx

DOI: 10.1039/x0xx00000x

www.rsc.org/

Miao Kan,[a] Jinping Jia[a] and Yixin Zhao[a]*

Here we report a high performance nanoporous silicon photoelectrode deposited with earth abundant $[Mo_3S_{13}]^{2-}$ nanoclusters for hydrogen generation. The earth aboudant $[Mo_3S_{13}]^{2-}$ nanoclusters with controllable loading can be facilely deposited onto nanoporous Si via drop coating of the monodispersed $[Mo_3S_{13}]^{2-}$ suspension following by drying. The nanoporous Si photoelectrode exhibited ~ 200 mV lower onset potential for photocurrent by reducing the interface resistance for hydrogen generation. The deposition of $[Mo_3S_{13}]^{2-}$ also passivate the nanoporous Si with a more stable photocurrent for hydrogen generation than b-Si in 20000 sec test.

Introduction:

Advanced technologies such photovoltaics and water splitting etc using sunlight to provide renewable energy have attracted more and more attention as an potential approach to address the environmental and energy crisis that threatening the prospect of human beings.[1-3] Among them, generating chemical fuel such as H_2 through direct photoelectrochemical (PEC) processes using sunlight becomes one of most promising sustainable energy candidates because hydrogen can facilely fit into current energy system for combustion engine or fuel cell electricity generation. [4, 5] A proper photoelectrode with suitable band gap and high activities of electrochemical catalysis are the most important factor for an efficient PEC hydrogen generation. Silicon is one of the most widely used candidate for photovoltaic and PEC due to its abundance and low cost although its 1.1 eV indirect band gap is not ideal for both applications. The decreasing cost and rapid development of PEC technique have made Si one of most popular photocathode candidates for PEC hydrogen generation.[6-10]

The performance of silicon photocathode for hydrogen generation is mainly limited by one challenges. The relatively low electrochemical activities of silicon for hydrogen generation although its conduction band is high enough for hydrogen production. To improve the PEC performance of silicon photocathodes, several strategies have been adopted to address these two challenges. The most popular way to improve Si photoelectrode's PEC performance is to enhance its electronic properties by nano engineering or forming heterjunction. Several types of Si nanostructures such as Si nanopores and nanowires have been fabricated to trap more light.[11-16] To further increase nanostructured Si photoelectrodes' PEC performance, the simplest way is to deposit different kinds of co-catalysts onto Si for hydrogen production.[17-24] Currently, the most active and popular co-catalysts is the well-known electrochemical catalysts of Pt, but the high cost and low abundance of Pt limit its large scale application. It's obliged to find a low cost Pt-alternative co-catalysts with advantages of high abundance and easy-to-synthesis. The popular candidates include MoS_2, MoS_x and Ni-Mo alloys etc.[25] The deposition of Pt or Pt alternative co-catalyst on to Si could be electrochemical deposition, electroless deposition, some physical deposition including sputtering and advanced deposition approaches such as ALD (atomic layer deposition), which also limit their fabrication. The simplest drop coating approach is usually ineffective for the co-catalyst deposition for Si photoelectrode due to the low contact between co-catalysts and Si. It would be ideal to have a facile drop coating co-catalyzed Si photoelectrode with high performance. The monodispersed 2-D MoS_2 nanosheet has been reported as an effective drop coating catalyst but its synthesis is complicated and the use of highly hazard chemicals such as lithium alkyls limits its application.[26-30] Here, we reported a high performance nanoporous silicon photoelectrode co-catalyzed by a low cost and easy-to-make earth abundant $(NH_4)_2Mo_3S_{13}.nH_2O$ nanocluster via a simple drop coating and drying.

Experimental Details:

Si wafers (B-doped, <100> oriented, 3-5 ohm) were first fabricated into planar Si photoelectrodes sealed with epoxy

[a] School of Environmental Science and Engineering
Shanghai Jiao Tong University
800 Dongchuan Road, Shanghai 200240 (China)
E-mail: yixin.zhao@sjtu.edu.cn

† Footnotes relating to the title and/or authors should appear here.
Electronic Supplementary Information (ESI) available: [details of any supplementary information available should be included here]. See DOI: 10.1039/x0xx00000x

with around 0.5cm^2 exposure area as previous reported.[31, 32] These planar Si photoelectrode was then processed into nanoporous Si photoelectrode via a metal-assisted chemical etching.[13, 33-36] The planar Si electrode was first electrolessly deposited with Ag by soaking in a solution consisting 1mM $AgNO_3$ and 1wt% HF for 30s, then washed with deionized (DI) water and blow dried with clean Ar. Then it was transferred into an etching solution with 31:6:364 volume ratio of 40% HF , 30wt% H_2O_2 and DI water for 6 min. The prepared nanoporous Si electrodes were then soaked in a 5M HNO_3 for 6 min to remove the Ag residue and then etched with 5% HF for 1 min followed by rinsed with DI water and dried with Ar. The nanoporous Si photoelectrode was then denoted as b-Si while the planar Si is denoted as pl-Si.

The $(NH_4)_2Mo_3S_{13}\cdot nH_2O$ was obtained by a Müller method as following procedure.[37, 38] 4.0g $(NH_4)_6Mo_7S_{24}\cdot nH_2O$ was dissolved in 20ml DI water in a conical flask. Then 120ml ammonium polysulfide solution (Xiya Reagent) was slowly added without stirring. The mixture solution was heated at 95℃ for 6h. After cooling down, the brown sediments were collected by centrifugation of the solution followed by washing with toluene, carbon disulfide and water. Finally, the red crystals were extracted were dispersed in DI water by mechanical oscillation and ready to be used. And the concentration of $[Mo_3S_{13}]^{2-}$ solution is determined by ICP-AES. The different amount of $[Mo_3S_{13}]^{2-}$ solution was drop cast onto pl-Si and b-Si photoelectrodes' surface and slowly dried in a 60℃ oven. Here the $[Mo_3S_{13}]^{2-}$ deposited planar Si and nanoporous Si are denoted as $[Mo_3S_{13}]^{2-}$/pl-Si and $[Mo_3S_{13}]^{2-}$/b-Si.

The morphologies of b-Si and $[Mo_3S_{13}]^{2-}$/b-Si were characterized by scanning electron microscopy (SEM, Nova nanoSEM450, FEI). The reflectance of b-Si photoelectrodes was characterized by UV-vis-NIR (Lambda 750, E.P.). The PEC measurement of pl-Si, b-Si, $[Mo_3S_{13}]^{2-}$/pl-Si and $[Mo_3S_{13}]^{2-}$/b-Si were carried out in pH=1.6 0.2 M phosphate buffer solution containing 0.5 M Na_2SO_4 using electrochemical workstations (CHI660E, CH Instrument and GAMRY)[39]. In all electrochemical measurements, different Si photolectrode, a Pt wire counter electrode and Ag/AgCl (3M KCl) reference electrode was placed in a three-electrode configuration irradiated with a white light halide lamp with 100mW/cm^2 (calibrated by CEL-NP2000). In a typical J-V experiment, the potential was swept from 0.2 to -1 V vs Ag/AgCl at a scanning rate of 50 mV/s. The reference electrode used in the experiment was Ag/AgCl (3M KCl), the potential of reversible hydrogen electrode (RHE) was calculated by following previous report.[40]

Results and Discussions:

The normalized X-ray diffraction (XRD) patterns of the ammonium thiomolybdate powder purified with CS_2 is listed in Fig.1a, which matches with the standard XRD patterns for $(NH_4)_2Mo_3S_{13}\cdot nH_2O$ (JCPDS:76-2038). The relative lower intensity of (111) peak suggests the obtained powder's crystal growth exhibits orientation preference. Interestingly, XRD pattern of as synthesized ammonium thiomolybdate powder sample is different from the purified one. First of all, the peak intensity of as synthesized $(NH_4)_2Mo_3S_{13}\cdot nH_2O$ is weak, suggesting a lower crystalline. Second, the as synthesized sample exhibited all typical XRD peaks of the $(NH_4)_2Mo_3S_{13}\cdot nH_2O$, which has much less crystal growth orientation as the purified one. The reason could be due to the sulfur residues (JCPDS:08-0799) shown in Fig. S4 because the CS_2 purification process could efficiently remove the excess sulfur residues. The less crystal orientation preference with excess sulfur could be attribute that the sulfur residue might work as can random nucleating sites to promote the crystallization process. After purified with CS_2, the $(NH_4)_2Mo_3S_{13}\cdot nH_2O$ can be well dispersed in alcohol solution with a yellowish colour and its UV-vis spectrum is listed in Figure 1b. This suspension is stable for days but the $(NH_4)_2Mo_3S_{13}\cdot nH_2O$ crystal will slowly precipitate during the storage and these dark

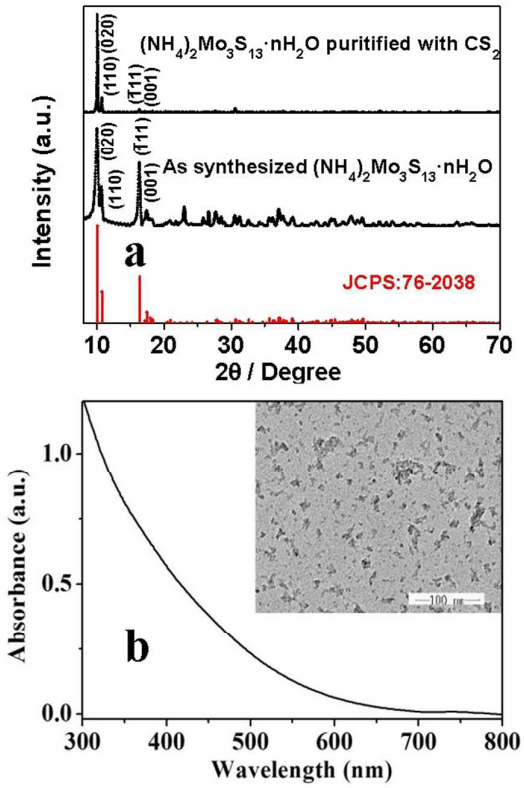

Figure 1 a) X-ray diffraction (XRD) pattern of as synthesized and purified ammonium thiomolybdate compared with standard $[(NH_4)_2Mo_3S_{13}].nH_2O$ (76-2038 and 08-0799), b) UV-vis spectrum and transmission electron microscope (TEM) image of ammonium thiomolybdate $[Mo_3S_{13}]^{2-}$ nanocluster suspension.

brown precipitates cannot be dissolve or re-dispersed. As a result, all the $(NH_4)_2Mo_3S_{13}\cdot nH_2O$ suspension is prepared freshly with CS_2 purification process. The transmission electron microscope (TEM) image of the fresh $(NH_4)_2Mo_3S_{13}\cdot nH_2O$ suspension is shown in Fig. 1 b, which revealed that the particle size of $(NH_4)_2Mo_3S_{13}\cdot nH_2O$ crystal varied from 5-30 nm with random morphologies.

The SEM image in Figure 2a reveals the morphology of nanoporous b-Si via metal assisted etching, the rough surface is full of ~100 nm nanopores holes as deep as 0.5μm. These nanopores could provide enough surface area for drop coating of $[Mo_3S_{13}]^{2-}$ nanocluster. The most of nanoporous b-Si photoelectrode's surface is covered by $[Mo_3S_{13}]^{2-}$ nanoclusters after the drop coating as shown in Figure 2b, and the EDS elemental mapping of Mo, N, S and Si is listed in Fig.2c, which suggests that the $[Mo_3S_{13}]^{2-}$ nanoclusters are mainly distributed on the Si surface not in the nanopores. The XPS of the $[Mo_3S_{13}]^{2-}$ nanoclusters deposited b-Si in Figure S1 are consistent with these EDX results. These $[Mo_3S_{13}]^{2-}$ nanocluster aggregated into large particles even exhibited a morphology of layer, which is different from their character of particle shown in Figure 1b. The plausible reason is that the $[Mo_3S_{13}]^{2-}$ nanocluster crystallize into large crystals assisted by the rough surface of b-Si. The cross-section SEM images in Figure 2b reveal that there is not much $[Mo_3S_{13}]^{2-}$ nanocluster penetrated into the nanopores, which is similar to the electroless deposited Pt as previous report.[31] These results revealed that the $[Mo_3S_{13}]^{2-}$ nanocluster can be homogenously deposited onto nanoporous Si photoelectrode via facile drop coating. These deposited $[Mo_3S_{13}]^{2-}$ nanoclusters are stable with Si and do not exhibit any electrochemical reaction under dark as confirmed by nearly zero dark current for all the $[Mo_3S_{13}]^{2-}$ nanoclusters co-catalysed b-Si photoelectrode. The PEC measurement further confirmed that these drop coating deposited $[Mo_3S_{13}]^{2-}$ nanoclusters can not only catalyse b-Si photoelectrode but also works on the pl-Si. Since negligible amount of $[Mo_3S_{13}]^{2-}$ nanoclusters is found the electrolyte solution after the J-V curve measurement, we assumed that the most drop coated $[Mo_3S_{13}]^{2-}$ nanoclusters effectively deposited stick onto Si surface.

To optimized the deposition loading of $[Mo_3S_{13}]^{2-}$ nanoclusters on b-Si photoelectrode, we had tried a serials of different amount $[Mo_3S_{13}]^{2-}$ nanoclusters loading in drop coating as shown in Figure S2. The photocurrent and onset potential for photocurrent all first increase then decrease with the loading of $[Mo_3S_{13}]^{2-}$ nanoclusters as shown in Figure S2. This trend suggests that the too much of $[Mo_3S_{13}]^{2-}$ nanoclusters loading could deteriorate the b-Si photoelectrode due to the light blocking or increase the interface resistance. The optimal $[Mo_3S_{13}]^{2-}$ nanoclusters loading density is found to be 100 nmol/cm^2, which exhibited a high photocurrent and low onset potential for photocurrent. Here we had to state that the area used for loading density is the project area of b-Si photoelectrodes rather than their real surfaces. The photocurrents can be assigned to the hydrogen evolution reaction,[24, 41] which has been confirmed by GC measurement with more than 98% faraday efficiency.

The representative PEC J-V curves of $[Mo_3S_{13}]^{2-}$/b-Si and $[Mo_3S_{13}]^{2-}$/pl-Si photoelectrodes compared with bare pl-Si and b-Si were shown in Fig.3 a. The photocurrent onset of pl-Si started around -0.7 V vs RHE with a ~22 mA/cm^2 photocurrent, which is consisted with previous reports. For simplification, we also drop coated 100 nmol/cm^2 $[Mo_3S_{13}]^{2-}$ nanoclusters onto pl-Si, the onset potential was then shifted to ~0 V vs RHE. Furthermore, there is no obvious photocurrent fluctuation found for the $[Mo_3S_{13}]^{2-}$/pl-Si while the regular pl-Si or Pt/pl-Si all exhibited serious photocurrent fluctuation. It is believed that the deposited $[Mo_3S_{13}]^{2-}$ nanoclusters provide enough active site for releasing hydrogen bubble. The b-Si photoelectrode is well known to exhibit a lower photocurrent onset potential than regular pl-Si because of its more active sites, here the photocurrent onset potential of bare b-Si is ~0 V vs RHE.[14]The b-Si could also show a high photocurrent than pl-Si due to the anti-reflection properties of b-Si. The Figure 3b illustrates the b-Si only reflect about 10% light while the pl-Si reflect about 30% light, which is consisted with the ~ 26 mA/cm^2 of b-Si compared with ~ 22 mA/cm^2 of pl-Si.[42] Once b-Si photoelectrode deposited with $[Mo_3S_{13}]^{2-}$ nanoclusters, its onset potential for photocurrent lower to + 0.2 V vs RHE, which is ~ 200mV lower than the bare b-Si. However, the photocurrent of $[Mo_3S_{13}]^{2-}$/pl-Si exhibited decrease in photocurrent compare to bare b-Si due to the plausible light block of $[Mo_3S_{13}]^{2-}$ or the increase of charge recombination.[31] The reflectance properties illustrated in Figure 3b revealed that the deposited $[Mo_3S_{13}]^{2-}$ nanoclusters could increase some light reflectance, which is consistent with the more smooth surface of b-Si after $[Mo_3S_{13}]^{2-}$ nanoclusters deposition. In all, the enhanced PEC performance of $[Mo_3S_{13}]^{2-}$/pl-Si is comparable to previous reported Pt/b-Si.[17, 31, 43]Figure 4c compares the EIS curves of different Si photoelectrodes in pH 1.6 buffer solution under 10mW/cm^2 irradiation at potential 0 V vs RHE. These Nyquist plots revealed that the deposition of $[Mo_3S_{13}]^{2-}$ nanocluster has significantly lowered the surface resistance of $[Mo_3S_{13}]^{2-}$/b-Si

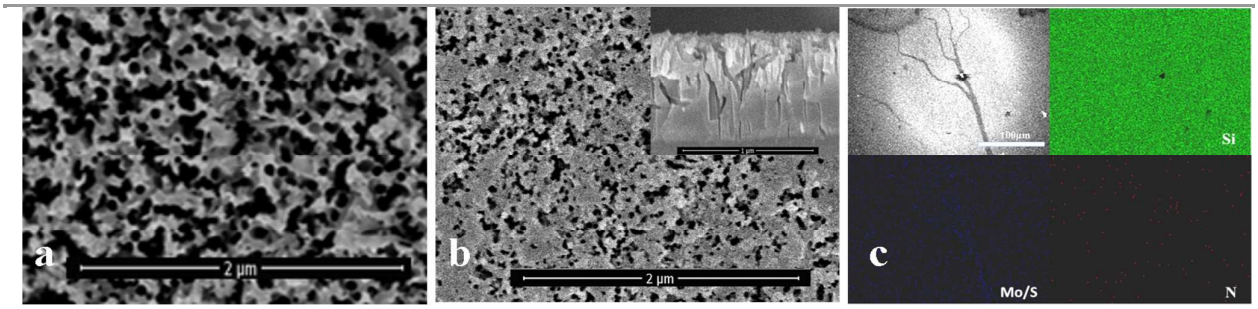

Figure 2 (a) SEM image of as prepared nanoporous silicon; (b) Top-view SEM image of $[Mo_3S_{13}]^{2-}$ deposited nanoporous silicon, inset is the cross-section view SEM image; (c) Elemental mapping of $[Mo_3S_{13}]^{2-}$ deposited nanoporous silicon.

(~470 Ω) compared to the bare b-Si photoelectrode (~1600Ω). The 20000 sec i-t curves of the bare b-Si and $[Mo_3S_{13}]^{2-}$/b-Si photoelectrodes are listed in Figure 3d. Both photoelectrode exhibited the degradation although the $[Mo_3S_{13}]^{2-}$/b-Si show some improvement. After the test, onset potential the J-V curves of both photoelectrodes go worse as shown in Fig S5.

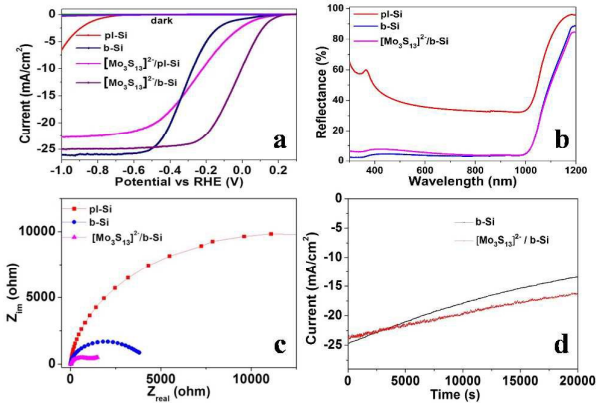

Figure 3 (a) J-V curves of different Si photoelectrodes in pH 1.6 solution under 100mW/cm^2 irradiation; (b) UV-vis-NIR reflectance of the different Si photoelectrodes; (c) Electrochemical impedance spectra comparison of different Si electrodes in pH 1.6 solution under 10 mW/cm^2 irradiation at 0 V vs AgCl/Ag; (d) I-t curves of the bare b-Si and $[Mo_3S_{13}]^{2-}$/b-Si in pH 1.6 solution under 100mW/cm^2 irradiation at -0.8 V vs RHE.

Conclusions

In summary, metal assisted etching prepared nanoporous b-Si could be facilely modified with earth abundant $[Mo_3S_{13}]^{2-}$ co-catalysts via a convenient drop coating and drying method with controllable deposition loadings. The $[Mo_3S_{13}]^{2-}$/b-Si exhibited improved PEC performance compared to bare b-Si. The enhanced PEC performance of $[Mo_3S_{13}]^{2-}$/b-Si was ascribed to the better charge transfer after $[Mo_3S_{13}]^{2-}$ deposition. Furthermore, the $[Mo_3S_{13}]^{2-}$ deposition not only lower the surface resistance for hydrogenation but also hold the photocurrent better than b-Si. In all, the earth abundant $[Mo_3S_{13}]^{2-}$ nanocluster is a potential co-catalyst with highly catalytic activities for PEC application.

Acknowledgement

YZ is thankful for the support of the NSFC (Grant 51372151 and 21303103).

Notes and references

1. D. Pimentel, L. Hurd, A. Bellotti, M. Forster, I. Oka, O. Sholes and R. Whitman, *Science*, 1973, **182**, 443-449.
2. M. Dresselhaus and I. Thomas, *Nature*, 2001, **414**, 332-337.
3. K. O. Ott, *Nuclear energy: a sensible alternative*, Springer Science & Business Media, 2012.
4. K. Mazloomi and C. Gomes, *Renew. Sust. Energ. Rev*, 2012, **16**, 3024-3033.
5. C. J. Winter and J. Nitsch, *Hydrogen as an energy carrier: technologies, systems, economy*, Springer Science & Business Media, 2012.
6. S. W. Boettcher, E. L. Warren, M. C. Putnam, E. A. Santori, D. Turner-Evans, M. D. Kelzenberg, M. G. Walter, J. R. McKone, B. S. Brunschwig and H. A. Atwater, *J. Am. Chem. Soc.*, 2011, **133**, 1216-1219.
7. D. H. Grantham, *Angew. Chem. Int. Ed. Engl.*, 1980.
8. S. Ida, K. Yamada, M. Matsuka, H. Hagiwara and T. Ishihara, *Electrochim. Acta*, 2012, **82**, 397-401.
9. V. Lehmann, *Electrochemistry of silicon: instrumentation, science, materials and applications*, 2002.
10. J. Zhao, A. Wang, M. A. Green and F. Ferrazza, *Appl. Phys. Lett*, 1998, **73**, 1991-1993.
11. A. P. Goodey, S. M. Eichfeld, K.-K. Lew, J. M. Redwing and T. E. Mallouk, *J. Am. Chem. Soc.*, 2007, **129**, 12344-12345.
12. I. Oh, J. Kye and S. Hwang, *Nano Lett.*, 2011, **12**, 298-302.
13. M. JináChoi and J. HoáBang, *J. Mater. Chem. A*, 2014, **2**, 833-842.
14. J. Oh, T. G. Deutsch, H.-C. Yuan and H. M. Branz, *Energy Environ. Sci*, 2011, **4**, 1690-1694.
15. S. Moniz, S. A. Shevlin, D. Martin, Z. Guo and J. Tang, *Energy Environ. Sci*, 2015.
16. E. L. Warren, J. R. McKone, H. A. Atwater, H. B. Gray and N. S. Lewis, *Energy Environ. Sci*, 2012, **5**, 9653-9661.
17. P. Dai, J. Xie, M. T. Mayer, X. Yang, J. Zhan and D. Wang, *Angew. Chem*, 2013, **125**, 11325-11329.
18. J. Feng, M. Gong, M. J. Kenney, J. Z. Wu, B. Zhang, Y. G. Li and H. J. Dai, *Nano Res.*, 2015, **8**, 1577-1583.
19. Y. Hou, B. L. Abrams, P. C. Vesborg, M. E. Björketun, K. Herbst, L. Bech, A. M. Setti, C. D. Damsgaard, T. Pedersen and O. Hansen, *Nat. Mater*, 2011, **10**, 434-438.
20. A. Morozan, V. Goellner, A. Zitolo, E. Fonda, B. Donnadieu, D. Jones and F. Jaouen, *Phys. Chem. Chem. Phys*, 2015.
21. F. F. Abdi, L. Han, A. H. Smets, M. Zeman, B. Dam and R. van de Krol, *Nat. Commn*, 2013, **4**.
22. B. Seger, A. B. Laursen, P. C. Vesborg, T. Pedersen, O. Hansen, S. Dahl and I. Chorkendorff, *Angew. Chem. Int. Ed.*, 2012, **51**, 9128-9131.
23. A. J. Nozik, *Annu. Rev. Phys. Chem.*, 1978, **29**, 189-222.
24. M. G. Walter, E. L. Warren, J. R. McKone, S. W. Boettcher, Q. Mi, E. A. Santori and N. S. Lewis, *Chem. Rev*, 2010, **110**, 6446-6473.
25. J. R. McKone, E. L. Warren, M. J. Bierman, S. W. Boettcher, B. S. Brunschwig, N. S. Lewis and H. B. Gray, *Energy Environ. Sci.*, 2011, **4**, 3573-3583.
26. B. Hinnemann, P. G. Moses, J. Bonde, K. P. Jørgensen, J. H. Nielsen, S. Horch, I. Chorkendorff and J. K. Nørskov, *J. Am. Chem. Soc.*, 2005, **127**, 5308-5309.
27. S. S. Chou, M. De, J. Kim, S. Byun, C. Dykstra, J. Yu, J. Huang and V. P. Dravid, *J. Am. Chem. Soc.*, 2013, **135**, 4584-4587.
28. Q. Ding, F. Meng, C. R. English, M. Cabán-Acevedo, M. J. Shearer, D. Liang, A. S. Daniel, R. J. Hamers and S. Jin, *J. Am. Chem. Soc.*, 2014, **136**, 8504-8507.
29. D. Voiry, M. Salehi, R. Silva, T. Fujita, M. Chen, T. Asefa, V. B. Shenoy, G. Eda and M. Chhowalla, *Nano Lett.*, 2013, **13**, 6222-6227.

30. S. Wu, Z. Zeng, Q. He, Z. Wang, S. J. Wang, Y. Du, Z. Yin, X. Sun, W. Chen and H. Zhang, *Small*, 2012, **8**, 2264-2270.
31. Y. Zhao, N. C. Anderson, K. Zhu, J. A. Aguiar, J. A. Seabold, J. v. d. Lagemaat, H. Branz, N. Neale and J. Oh, *Nano Lett.*, 2015, **15**, 2517-2525.
32. M. Kan, D. Yue, J. Jia and Y. Zhao, *Electrochim. Acta*, 2015.
33. Z. Huang, N. Geyer, L. Liu, M. Li and P. Zhong, *Nanotechnology*, 2010, **21**, 465301.
34. X. Li and P. Bohn, *Appl. Phys. Lett*, 2000, **77**, 2572-2574.
35. Z. Huang, N. Geyer, P. Werner, J. De Boor and U. Gösele, *Adv. Mater*, 2011, **23**, 285-308.
36. U. Sim, H.-Y. Jeong, T.-Y. Yang and K. T. Nam, *J. Mater. Chem. A*, 2013, **1**, 5414-5422.
37. A. Müller, S. Sarkar, R. G. Bhattacharyya, S. Pohl and M. Dartmann, *Angew. Chem. Int. Ed.*, 1978, **17**, 535-535.
38. J. Kibsgaard, T. F. Jaramillo and F. Besenbacher, *Nat. Chem*, 2014, **6**, 248-253.
39. Z. Huang, P. Zhong, C. Wang, X. Zhang and C. Zhang, *ACS Appl. Mat. Interfaces*, 2013, **5**, 1961-1966.
40. N. P. Dasgupta, C. Liu, S. Andrews, F. B. Prinz and P. Yang, *J. Am. Chem. Soc.*, 2013, **135**, 12932-12935.
41. M. G. Walter, E. L. Warren, J. R. McKone, S. W. Boettcher, Q. Mi, E. A. Santori and N. S. Lewis, *Chem. Rev*, 2011, **111**, 5815-5815.
42. J. D. Benck, T. R. Hellstern, J. Kibsgaard, P. Chakthranont and T. F. Jaramillo, *ACS Catal.* , 2014, **4**, 3957-3971.
43. K. Peng, X. Wang, X. Wu and S. T. Lee, *Nano Lett.*, 2009, **9**, 3704-3709.

TOC

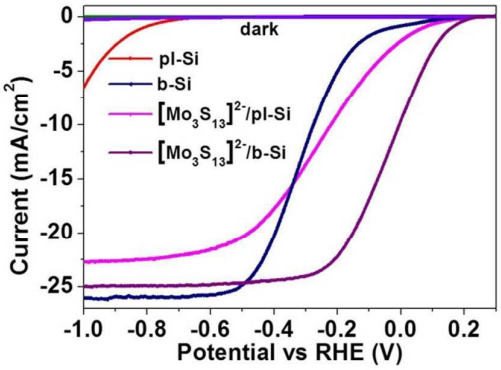

The earth abundant $[Mo_3S_{13}]^{2-}$ nanoclusters efficiently enhance nanoporous silicon photoelectrode for hydrogen generation.